Structural Durability & Health Monitoring

Tech Science Press

https://doi.org/10.32604/sdhm.2026.072074

ARTICLE

Numerical Research on Multi-Directinal Deformation Control of Shield Tunnels under Surface Surcharge

Pengfei Zhao[1,*] **and Youlin Ye**[2]

[1]China Railway 15 Bureau Group Urban Rail Transit Engineering Co, Ltd., Guangzhou, China
[2]School of Transportation and Geomatics Engineering, Shenyang Jianzhu University, Shenyang, China

*Corresponding Author: Pengfei Zhao. Email: zhaopengfei1990@126.com

Received: 19 August 2025; Accepted: 28 October 2025; Published: 18 May 2026

ABSTRACT: Under soft soil geological conditions, tunnel engineering disturbances can induce changes in ground surface surcharges and lead to stress redistribution in the surrounding soils. As relatively unfavorable loads during engineering disturbances, ground surface surcharges significantly influence both transverse and longitudinal deformations of shield tunnel structures, resulting in increased ellipticity, segment dislocations, joint openings, and tunnel settlement. This study investigates the effect of two different steel plate reinforcement methods—annular steel plates and cross-joint steel plates—on tunnel structures under surface surcharge loading. Using the Mohr–Coulomb elastoplastic constitutive model, the influence of surface surcharges on shield tunnel segment deformation and adjacent soil behavior is analyzed. Numerical modeling is performed based on surface loading parameters obtained from the river channel section of Metro Line 9 in an eastern region of China, and the model is validated through correlation between finite element analysis results and measured tunnel settlement data. The results indicate that annular steel plates exhibit effectiveness comparable to that of cross-joint steel plates in controlling tunnel ovalization and circumferential joint separation under surface surcharge conditions. However, cross-joint steel plates perform better in mitigating longitudinal deformations of the tunnel, including differential settlement and vertical displacement. In addition, cross-joint steel plates demonstrate a stronger capacity to control shear stress distribution within tunnel segments compared to annular configurations. These findings provide valuable references for shield tunnel engineering in load-disturbed environments.

KEYWORDS: Ground surface surcharge; transverse and longitudinal deformations; reinforcement of steel plates; numerical simulation

1 Introduction

During the operation of shield tunnels, disturbances from external factors or engineering activities, such as ground surcharges and foundation pit excavation near tunnels, increase the risk of tunnel structural deformation [1]. To cope with such engineering disturbances, it is necessary to accurately measure the stress and deformation conditions of tunnels and surrounding soils and select an appropriate reinforcement method.

In order to study the engineering disturbances in tunnels in ground surface surcharges and cause stress redistribution in the soils surrounding the tunnels, scholars have done a lot of research. Huang et al. [2] established a three-dimensional model of a shallow shield tunnel in soft soil to analyze the deformation response under sudden additional load. The results indicate that controlling the surcharge height is the most effective measure, with maximum surface settlement and tunnel vault settlement reduced by approximately 65% or more when the surcharge height is decreased from 6 to 2 m. Guang et al. [3] conducted a

laboratory-scale physical model test with a scaling factor of 1:15.5 to investigate the detrimental effects of abrupt surface surcharges on in-service shield tunnels. Han et al. [4] investigated the combined effects of surcharge and spatial variability of soil properties using a random finite element method. They found that tunnel deformation and surface settlement intensify with increased surcharge eccentricity/height and greater variability (COV & SOF) of the soil's elastic modulus. Wei et al. [5] employed advanced numerical modeling techniques to study the deformation behavior of shield tunnel linings subjected to surface surcharges. Through finite element analysis, they established a sophisticated 3D simulation that accurately captured the unique staggered assembly characteristics of precast concrete segments in shield tunnels. This computational approach enabled detailed investigation of structural responses under various loading scenarios. Xiang et al. [6] examined how bilateral surface loading and unloading conditions affect pre-existing shield tunnels at different overburden depths through comprehensive numerical analyses. Their research focused on evaluating structural responses under asymmetrical surface pressure variations, considering multiple embedment depth scenarios to determine depth-dependent behavior patterns. Yuan et al. [7] conducted an experimental study on a scaled-down model to investigate the impact of ground surcharge on a quasi-rectangular pipe jacking tunnel. They found that the structural response is primarily governed by the surcharge's eccentricity and the tunnel's burial depth, with shallow depths and zero/eccentric loads inducing distinct effects. Lee et al. [8] developed a novel analytical approach to evaluate how surrounding ground resistance and longitudinal joint characteristics (including spatial arrangement, number, and rigidity) affect the stress distribution and deformation patterns in tunnel lining structures. Their methodology specifically addressed the mechanical interaction between segmental joints and adjacent strata under operational conditions. Wu et al. [9] developed an innovative soil-tunnel interaction framework to evaluate the structural response of shield tunnels under surface-induced loading conditions. The researchers implemented this computational model to systematically examine how externally applied surcharges propagate through the ground medium and subsequently affect tunnel behavior. However, considering the structural complexity of tunnels in both the transverse and longitudinal directions, many scholars tend to simplify the joint contacts between segments and rings when simulating tunnel structures and investigating deformation mechanisms, which makes it difficult to accurately capture the actual stress state. At present, research on the deformation mechanisms of shield tunnels mainly focuses on individual segments, where the load–structure method is employed to simulate the mechanical interaction between the surrounding soil and the tunnel structure, while studies on longitudinal deformation of tunnel structures remain relatively limited.

To maintain tunnel structural integrity under external disturbances or construction impacts, proper strengthening techniques must be implemented. Liu et al. [10] conducted experimental investigations on full-scale lining specimens reinforced with steel plating to evaluate their maximum load-bearing performance. They demonstrated that adhering steel plates to deformed segments is a technically sound and feasible approach, which significantly improves the structural performance by increasing both load resistance and rigidity. Qin et al. [11] conducted a full-scale test to evaluate the mechanical behavior of deformed shield tunnels strengthened with stainless steel corrugated plates (SSCP). They demonstrated that the SSCP technique effectively enhances the tunnel's ultimate bearing capacity and stiffness, and proposed two methods to further improve its utilization. Liu et al. [12] conducted a comprehensive study on the failure behavior and reinforcement efficiency of corbel-equipped steel plate strengthened shield tunnel linings. In a related investigation [13], researchers employed both experimental testing and analytical modeling to evaluate the performance enhancement of tunnel lining structures when retrofitted with textile-reinforced concrete, particularly focusing on the improvement in flexural capacity. Oguz et al. [14] investigated the possibility of adopting glass fibre reinforced polymer and macro-synthetic fibres in metro tunnel segments. Gang et al. [15] performed extensive experimental research on three-ring staggered segment assemblies to

examine the mechanical response and strengthening performance of shield tunnel structures under ground loading disturbances in Hangzhou Metro projects. The investigation employed a custom-designed hydraulic loading apparatus specifically developed for tunnel segment testing, which enabled precise evaluation of structural behavior under simulated operational conditions. It is clear that previous studies have mainly focused on the reinforcement effects on the transverse deformation of tunnel segments; thus, limited reports on the efficacy of reinforcement measures in controlling the longitudinal deformation of tunnel structures are available. Moreover, most reinforcement studies have been conducted on tunnels that already experienced deformations. However, as deformed segments cannot be tested repeatedly, numerical simulations can effectively address this limitation.

In numerical simulations evaluating the effectiveness of tunnel reinforcement measures, the load-structure method is commonly employed. However, in soft soil regions, the nonlinear characteristics of soil are particularly pronounced. The load-structure method fails to accurately simulate soil deformation under ground surface surcharge conditions or the interactive deformation behavior between tunnels and surrounding soils. Moreover, the nonlinear deformations of soil vary significantly under different loading conditions. Therefore, based on the soft soil geological conditions in East China, the Mohr-Coulomb (MC) elastoplastic constitutive model was adopted in this study. A three-dimensional solid model of the river channel section of Metro Line 9 in a region of East China was developed using ABAQUS software, and the pre-strengthening effects of two types of steel plates (steel plates in rings and steel plates spanning circumferential joints) on the tunnel structure under ground surface surcharge conditions were analyzed. Fig. 1 presents the overall research framework of this article.

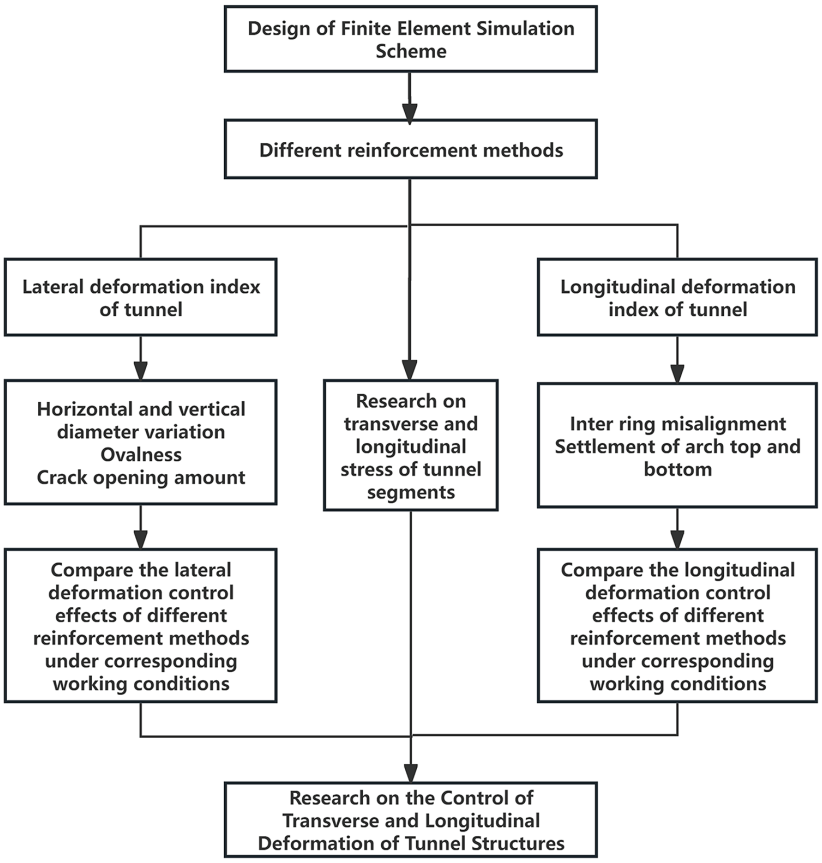

Figure 1: The overall research framework.

2 Constitutive Behavior and Contact Relationship of Materials

2.1 Mohr-Coulomb Model

The MC model provides a good idea of the shear failure of rocks and soils and can reflect the difference in the compressive and tensile strengths of soils. To facilitate convergence, a smoothing treatment was executed on the plastic potential function of the yield criterion for the MC model adopted in ABAQUS.

The yield function of the MC elastoplastic model was expressed in Mohr's form, as shown in Eq. (1):

$$\tau = c = \sigma \tan \varphi \tag{1}$$

σ (normal stress): This is the stress component perpendicular to the shear plane. It represents the compressive stress acting normal to the plane of potential failure. τ (shear stress): This is the stress component parallel to the shear plane. It represents the driving force for shear failure. φ (internal friction angle): This is an angle (in degrees) that characterizes the frictional resistance of the material. A higher φ indicates greater shear strength under normal stress, typical for dense soils or rocks. C (cohesion): This is the intercept of the shear strength envelope, representing the inherent shear strength of the material when normal stress is zero. It is due to chemical bonding or cohesion in soils. This equation defines the failure envelope in Mohr stress space: if the state of stress (σ, τ) lies above this line, failure occurs.

The Coulomb expression was shown in Eq. (2)

$$s + \sigma_{\mathrm{m}} \sin \varphi - c \cos \varphi = 0 \tag{2}$$

where $s = \frac{1}{2}(\sigma_1 - \sigma_3)$ and $\sigma_m = \frac{1}{2}(\sigma_1 + \sigma_3)$.

σ_1 (major principal stress): The maximum compressive stress. It is the largest principal stress in the system. σ_3 (minor principal stress): The minimum compressive stress. It is the smallest principal stress, which can be tensile in some cases. This expression is derived from Mohr's circle analysis and provides a failure criterion in terms of principal stresses, which are easier to measure in experiments.

The MC yield criterion assumes that a point will fail when the shear stress acting on it reaches its shear strength and the shear strength has a linear relationship with the normal stress acting on that plane. The MC model acts based on the stress state of materials at failure and uses Mohr's circles to describe the failure conditions under different stress combinations (Fig. 2).

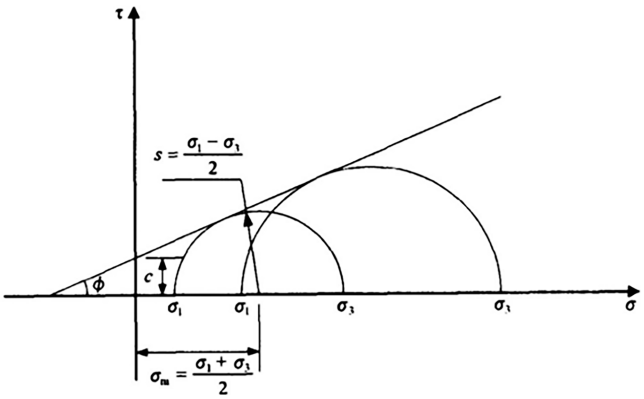

Figure 2: Mohr-Coulomb failure model.

The shear yield surface function of the MC model is shown in Eq. (3).

$$F = R_{\mathrm{mc}}\, q - p \tan \phi - c = 0 \tag{3}$$

where φ is the inclination angle of the MC yield surface on the $q - p$ stress plane (friction angle of the material), c is the cohesion of the material. The tensile failure criterion adopts the Rankine criterion, as shown in Eq. (4).

$$F_{\mathrm{t}} = R_{\mathrm{t}}\,(\Theta)\, q - p - \sigma_{\mathrm{t}} = 0 \tag{4}$$

where $R_{\tau}\,(\Theta) = 2/3 \cos\,(3\Theta)$, Θ is the polar deviation angle ($\cos\,(3\Theta) = r^3/q^3$), r is the third invariant of the deviatoric stress tensor J_3, $R_{mc}(\Theta, \varphi)$ controls the shape of the yield surface on the π-plane. And σ_{t} represents the tensile strength, which varies with the equivalent tensile plastic strain.

Fig. 3 presents the shapes of the MC yield surface on the meridian plane $(\Theta = 0)$ and the π-plane and illustrates its relationships with the Drucker-Prager yield surface, the Tresca yield surface, and the Mises yield surface.

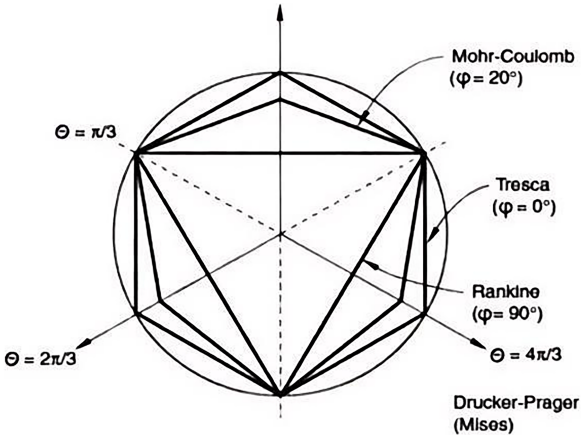

Figure 3: Yield surface of the Mohr-Coulomb model.

2.2 Contact Relationship

The interactions between the soil, the concrete segments, and the bolts were modeled and simulated by setting the contact relationships among them to understand their mechanical behaviors and mutual influences under actual conditions. In the finite element model, the concrete segments were realized using three-dimensional solid elements. The concrete segments were connected by transverse bolts, and the rings were connected by 17 longitudinal bolts. The shanks of the transverse and longitudinal bolts were modeled using B31 beam elements, and the nuts were simulated using S4R shell elements. These two bolt elements were embedded into the concrete segments to create a constraining effect. The steel plates were simulated using S4R shell elements. In the numerical simulation, the interaction between steel plates and concrete segments was characterized using constraint equations in ABAQUS, enabling the composite system to effectively transfer axial, shear, and compressive stresses while functioning as an integrated structural unit. The normal interaction at segment-to-segment and tunnel-to-soil interfaces was defined using a "hard contact" formulation, while tangential behavior was governed by a penalty friction model incorporating Coulomb's law. For concrete segment interfaces, a friction coefficient of 0.4 was implemented to properly represent the frictional characteristics [16]. The soil-tunnel interface employed a calculated friction coefficient of 0.27

derived from the soil's internal friction angle, with full friction mobilization permitted when contact surfaces were in compression.

3 Numerical Model

3.1 Establishment of a Three-Dimensional Finite Element Model of the Tunnel under Consideration

The stratigraphy in the Shanghai area is dominated by soft soil, primarily silty clay and muddy soil, with a high groundwater table. According to the ground surface surcharge example of the river channel of t Metro Line 9 in a region of East China, the river channel is located directly above an interval shield section of the Metro Line 9. During the construction of nearby projects, the riverbed has undergone backfilling operations. The height and unit weight of the backfilled soil are 4.5 m and 17 kN/m^3, respectively, and such a high gravity load of the backfilled soil causes an uneven settlement impact on the underlying shield tunnel. The river channel is 24 m wide and 3 m deep, and the distance from the riverbed to the top of the subway tunnel is 5 m (Fig. 4).

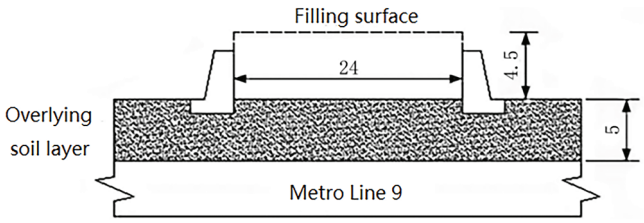

Figure 4: Relationship between the relative positions of the river channel and the tunnel.

Considering computational efficiency and observed symmetry in tunnel settlement patterns, the numerical simulation was strategically limited to the right-side region relative to the surcharge center (Fig. 5). The developed finite element model comprised 32 segmental rings, each 1.2 m wide, resulting in a total longitudinal dimension of 38.4 m. The model geometry included a 12 m wide filled soil zone on the left side, with overall soil dimensions of 38.4 m (length) × 20 m (width) × 20 m (height). The tunnel crown was positioned 5 m below ground surface. Surface loading conditions were simulated through equivalent pressure application, with an implemented value of 76.5 kPa representing the surcharge effect.

The numerical model implemented comprehensive boundary conditions to properly simulate the physical constraints of the system. The soil base was fully restrained with fixed supports in all three coordinate directions (x, y, and z), while lateral boundaries received x-direction constraints to represent adjacent soil continuity. Longitudinal restraint conditions were applied to both z-direction boundaries of the soil mass and the tunnel structure, effectively modeling the confined nature of the underground environment.

To accurately represent the behavior of the internal tension ring, the ring was modeled using S4R shell elements to capture the bending and membrane response of the thin-walled circular member. The interaction between the internal tension ring and the concrete segments was idealized using ABAQUS "tie" constraints, which effectively simulate the epoxy bonding and the shear transfer capacity of the expansion bolts. This tied interface enables simultaneous transfer of tensile, compressive and shear forces between the ring and the segments, forming a composite load-bearing system.

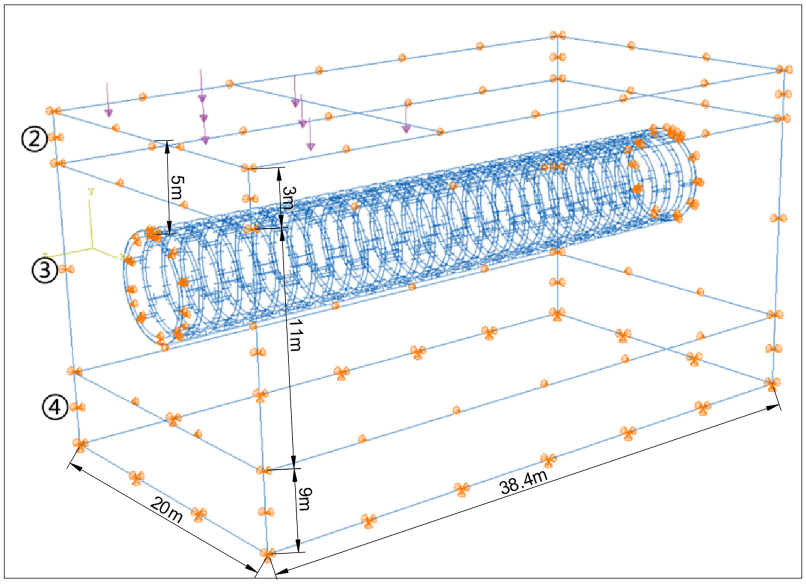

Figure 5: Finite element model of the tunnel.

3.2 Structural and Material Parameters

The numerical simulation incorporated detailed material properties, with tunnel segment characteristics specified in Table 1 and constituent material parameters provided in Table 2. Geotechnical properties of the river channel strata were documented in Table 3. Structural reinforcement elements included primary steel plates measuring 850 mm in width and 20 mm in thickness, complemented by longitudinal steel strips with dimensions of 100 mm width and equivalent 20 mm thickness.

Table 1: Tunnel segment parameters.

Tunnel Outer Diameter (m)	Segment Thickness (m)	Ring Width (m)	Number of Bolts (n)	Bolt Diameter (m)	Bolt Length (m)
6.2	0.35	1.2	17	0.03	0.4

Table 2: Tunnel material parameters.

Materials	Type	Elastic Modulus (GPa)	Poisson's Ratio	Yield Strength (MPa)
Segment lining	C55	35.5	0.2	25.3
Bolt	M30	210	0.3	400
Steel plate	Q235	200	0.3	235

Table 3: Physical and mechanical parameters of the soil layers.

Soil Layer	Thickness (m)	Unit Weight ($kN \cdot m^{-3}$)	Elastic Modulus (MPa)	Poisson's Ratio	Cohesion (kPa)	Internal Friction Angle (°)
Fill soil	4.5	17	–	–	–	–
②	3	18.7	15	0.31	22	18.5
③	11	17.2	9	0.33	13	15.5
④	9	16.7	6	0.33	14	10.5
⑤	6	19.4	21	0.30	45	15.5
⑥	14	19	36	0.29	3	31.5

4 Validation of the Ground Surface Surcharge Model and Setting up of Reinforcement Working Conditions

4.1 Validation of the Ground Surface Surcharge Model

Fig. 6 presents a comparative analysis between field-measured data and numerical simulation outcomes for the tunnel structure. The close correlation observed between predicted and actual values beneath the surface loading center demonstrates the model's validity and confirms its accuracy in representing the physical behavior of the tunnel system under surcharge conditions.

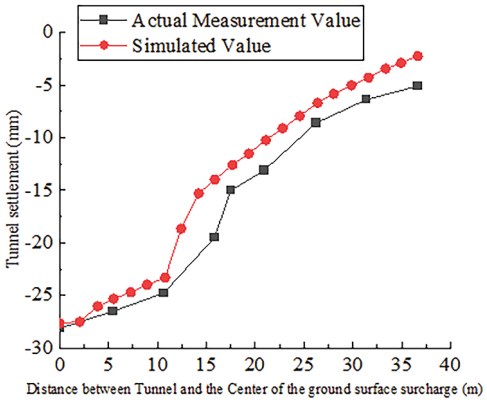

Figure 6: Comparison between the measured and numerical results of the tunnel.

To further explain the validation approach, it is noted that field monitoring for the present engineering case was focused on the surcharge center where the tunnel experiences the most significant and representative settlement response. Therefore, settlement at this critical section was selected as the primary benchmark for model validation. The close agreement between simulated and measured settlements at this location confirms the accuracy of the finite element model and the appropriateness of the adopted parameters. In future work, additional field monitoring data at multiple tunnel positions (including lateral deformation, longitudinal displacement, and stress distribution) will be incorporated to enhance cross-validation and improve model generality.

4.2 Reinforcement Setup

Two types of pre-strengthening methods were used in this analysis: Fig. 7 reinforcement of steel plates in the rings and Fig. 8 reinforcement of steel plates spanning circumferential joints. The connection between

the steel plates and the tunnel segments was realized using a bisphenol-A epoxy adhesive. Epoxy resin is a thermosetting polymer formed by the ring-opening crosslinking of epoxy groups with amine or anhydride curing agents, which creates a dense three-dimensional network providing both chemical adhesion and mechanical interlocking with the steel surface.

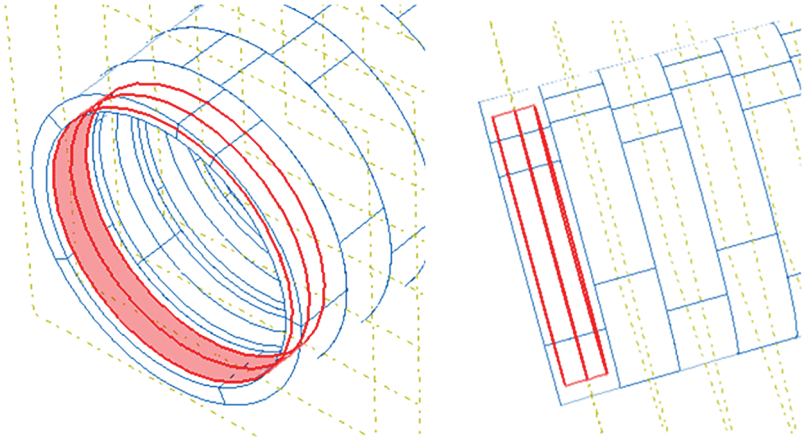

Figure 7: Reinforcement of steel plates in the rings.

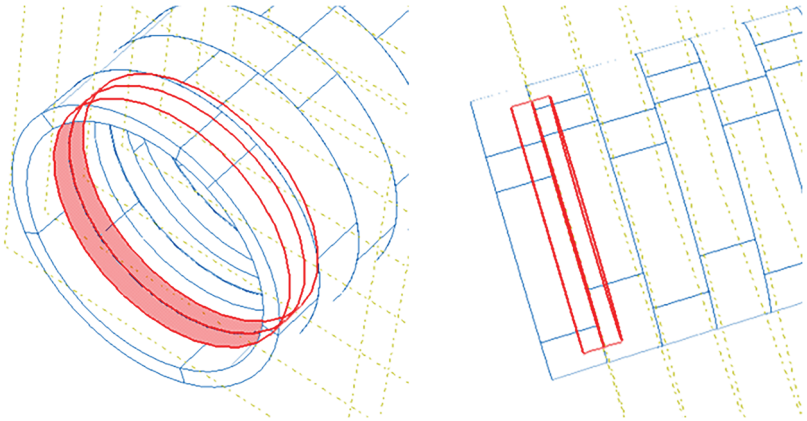

Figure 8: Reinforcement of steel plates spanning circumferential joints.

Prior to bonding, the steel plates were grit-blasted to Sa2.5 grade, and the concrete segment surfaces were ground and cleaned to ensure surface activation and proper wetting. The epoxy resin and curing agent were mixed at the manufacturer's recommended mass ratio (2:1) and cured at ambient temperature (20°C–25°C) for 48 h to achieve full polymerization; post-curing can be applied to increase the glass transition temperature if higher thermal resistance is required. Considering the humid and water-seepage environment of tunnels, a water-resistant modified epoxy system was selected to mitigate possible moisture absorption, plasticization, and strength reduction during long-term service. The bonding performance and durability of the adhesive were referenced against widely used international standards (e.g., ASTM D1002, ISO 4587), and engineering practice indicates that properly selected and applied epoxy joints can provide a design service life exceeding 20 years.

In the numerical model, the tunnel segments were described by the Mohr–Coulomb elastoplastic constitutive law to simulate shear and compressive failure, and the initial interface bonding strength of the

epoxy adhesive was calibrated using test data to represent the as-built performance. Long-term adhesive degradation can be further considered in future work through time-dependent reduction models for interface strength and fracture energy.

According to the technical regulations for the safety protection of urban rail transit structures [17], the value of additional loads on the outer wall of tunnel structures should be less than 20 kPa. Hence, four different ground surface surcharges of 30, 50, 76.5, and 100 kPa corresponding to fill soil heights of 1.76, 2.94, 4.5, and 5.88 m, respectively, were used. The additional load acting on the outer wall of the tunnel was approximately 0.65 times the ground surface surcharge.

5 Analysis of the Deformation Control Effects of the Two Reinforcement Methods

The deformation profiles of the tunnel without reinforcement and the soil under the ground surface surcharge of 76.5 kPa are displayed in Fig. 9. The deformation of the soil mainly occurred in the area near the ground surface surcharge center, and the tunnel under the soil mass also experienced significant transverse deformation and longitudinal settlement under the ground surface surcharge center. The strong influence zone of the longitudinal settlement existed within a range of 10 sections of the tunnel to the right of the ground surface surcharge center, suggesting that the strong influence zone of the longitudinal settlement was within a range of 12 m to the right of the ground surface surcharge center. The tunnel was significantly displaced in the ground surface surcharge area, and an uneven settlement with significant dislocations and joint openings between the segments occurred along the longitudinal direction of the tunnel.

5.1 Ellipticity Analysis

The effect of the transverse deformation control of the tunnel was described by the ellipticity of the tunnel segments. Ellipticity was described by the changes in the transverse and longitudinal diameters of the tunnel [18]:

$$Ellipticity = (a - b)/D$$

where D is the nominal outer diameter of the tunnel lining (unit: mm); a and b are the variation values of the transverse diameter (left–right direction) and longitudinal diameter (crown–invert direction) of the tunnel cross section (unit: mm). Here, "variation" is defined as the measured diameter minus the design diameter; thus, a positive a indicates that the horizontal diameter has increased, and a positive b indicates that the vertical diameter has increased.

For this study, the transverse and longitudinal diameters were obtained from the first ring of segments under the surcharge center by extracting coordinates at the crown, invert, and both haunches of the tunnel lining in the numerical model and corresponding monitoring data. Ellipticity is a dimensionless parameter: a value of zero indicates a circular section; a positive value indicates horizontal expansion and vertical shortening; and a negative value indicates the opposite trend. This index is widely used to quantify cross-sectional distortion of shield tunnels under ground loading and to evaluate the effectiveness of reinforcement measures in controlling transverse deformation.

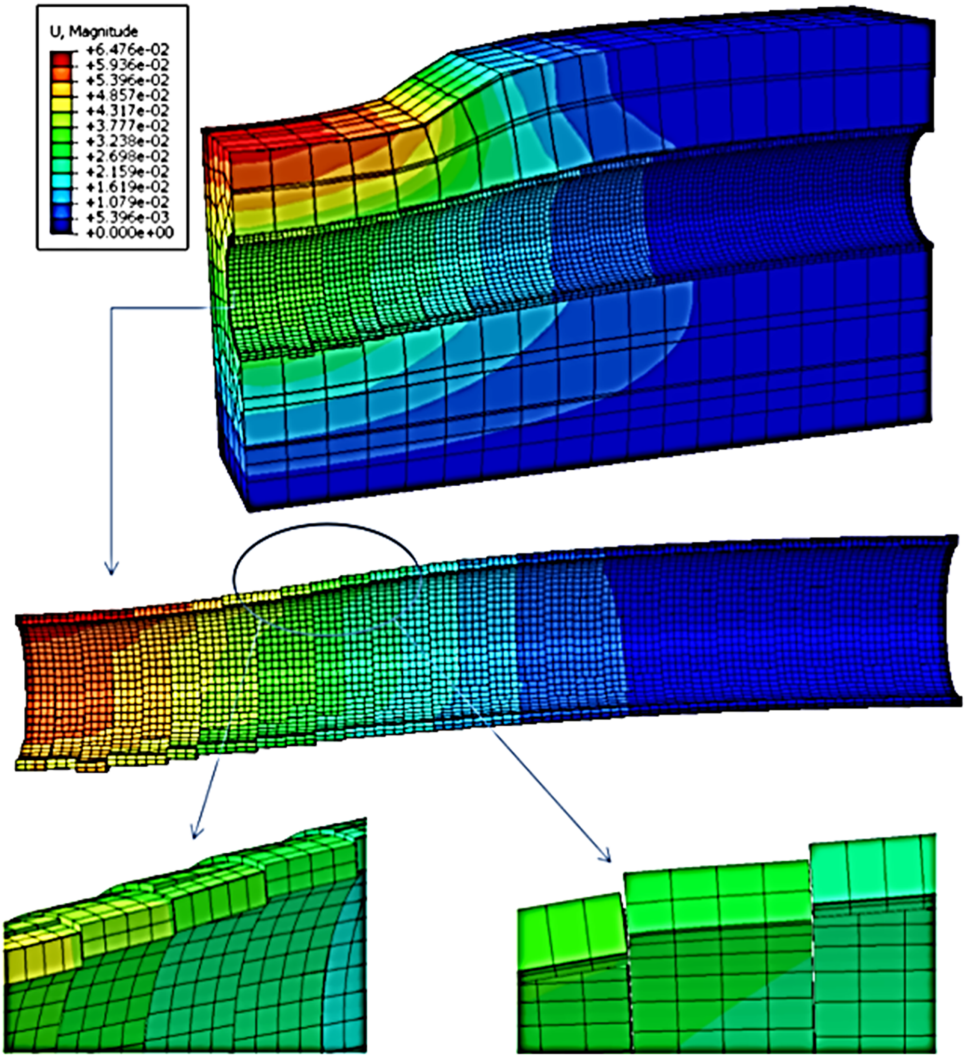

Figure 9: Deformation profiles of the soil and the tunnel without reinforcement under the ground surface surcharge of 76.5 kPa.

The first ring of the tunnel segments under the ground surface surcharge center was taken for the comparative analysis of the effects of ellipticity control under different reinforcement conditions. It is evident from Fig. 10 that when the ground surface surcharges were 30, 50 , 76.5, and 100 kPa, the ellipticity of the tunnel reinforced with steel plates in the rings was reduced by 65.69%, 66.26%, 66.98%, and 67.48%, respectively, in comparison to those of the unreinforced one. After the reinforcement of the tunnel with steel plates spanning circumferential joints, the corresponding values became 69.09%, 65.57%, 62.28%, and 60.61%, respectively.

It is discernible that both types of reinforcement had an obvious effect in controlling ellipticity. It is noticeable from Fig. 9 that at about 50 kPa, the control effects of both types of reinforcement were nearly the same. The steel plates in the rings and the steel plates spanning circumferential joints reduced the tunnel ellipticity by 66.60% and 64.39%, respectively. Moreover, both reinforcement techniques solved the transverse deformation problem of the tunnel.

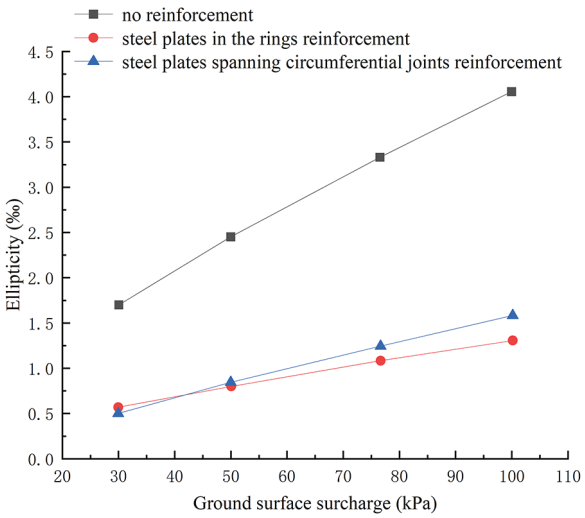

Figure 10: Comparison of ellipticity under different reinforcement conditions. Note: The figures present the absolute ellipticity values, whereas the text refers to the percentage reduction in ellipticity relative to the unreinforced case. Both are derived from the same dataset and are consistent in reflecting the deformation control effect of different reinforcement schemes.

5.2 Dislocation and Joint Opening Analysis

Dislocations and joint openings are the most common forms of longitudinal deformation in tunnel structures. If dislocations and joint openings are not controlled correctly, they can damage water-resisting strips between tunnel segments, resulting in water leakage, which reduces the longitudinal stiffness of tunnels and even causes the failure of longitudinal bolts. The amounts of dislocations and joint opening were measured between the top segments of the eighth and ninth rings of the tunnel and also between adjacent segments at the bottom center of the ground surface surcharge area (Fig. 11).

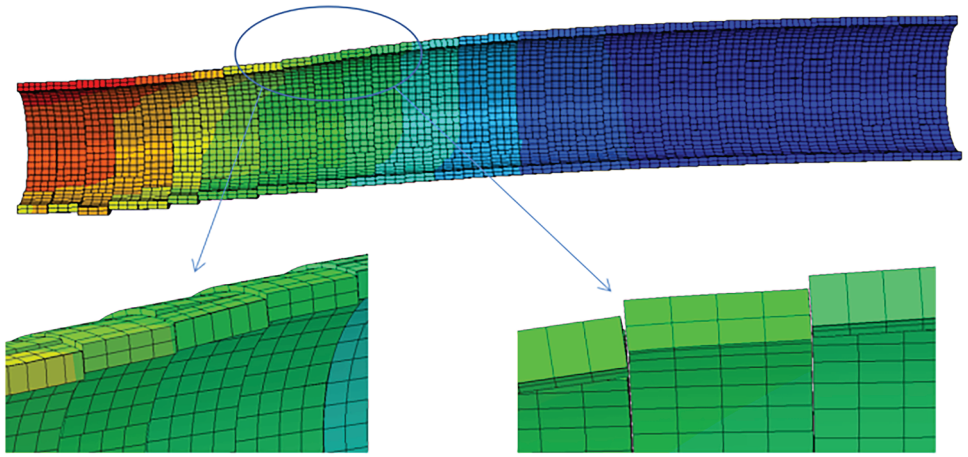

Figure 11: Dislocation and joint opening of the tunnel.

5.2.1 Dislocation Analysis

Fig. 12 clearly demonstrates the superior performance of cross-joint steel plate reinforcement in controlling tunnel dislocations compared to annular plate strengthening. Under surface loading conditions of 30, 50, 76.5, and 100 kPa, the annular plate configuration achieved dislocation reductions of 17.06%, 18.31%, 25.09%, and 29.35% respectively relative to unreinforced conditions. In contrast, circumferential joint reinforcement showed remarkable effectiveness in minimizing ovalization, achieving reduction rates of 91.67%, 87.63%, 88.98%, and 90.44% for the same loading increments when compared to unstrengthened tunnel sections.

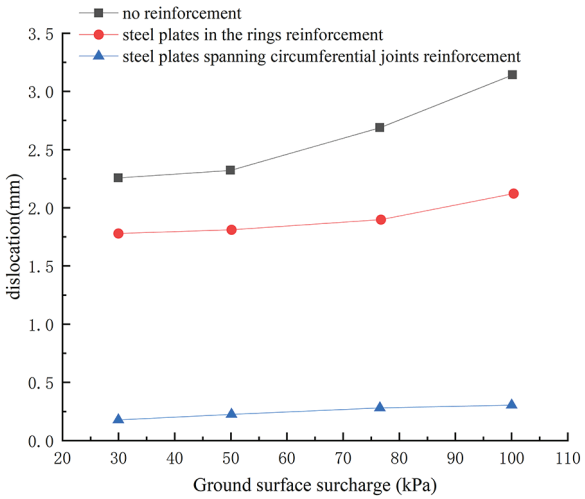

Figure 12: Comparison of dislocations under different dislocation conditions.

The remarkable dislocation reduction (over 90%) achieved by cross-joint steel plates is mainly due to their direct restraint on relative shear displacement and joint opening between adjacent rings. Cross-joint plates are installed across the circumferential joints and anchored by bolts or welding, creating a continuous load-transfer path that spreads local concentrated forces into neighboring segments and greatly enhances the shear stiffness of the ring-to-ring connection. From a structural mechanics perspective, this reinforcement acts as additional shear connectors in the weak joint region, significantly increasing the shear and bending resistance of the inter-ring interface, which explains the pronounced dislocation control.

In contrast, annular steel plates mainly reinforce the stiffness of each individual ring. They continuously strengthen the bending rigidity within a single ring but do not directly improve the mechanical interlocking and force transfer efficiency between rings. Since dislocation at joints is primarily governed by shear deformation and opening at the ring interfaces, annular plates have only moderate influence on inter-ring displacement reduction.

This difference aligns with basic joint mechanics and global structural response theory and is consistent with field engineering practice for joint reinforcement in shield tunnels.

The superior dislocation mitigation achieved with cross-joint steel plate reinforcement compared to annular plate installation stems from its strategic placement at inter-ring connections. This configuration significantly enhances both the axial rigidity of tunnel segments and the shear resistance across ring interfaces. Such effective dislocation management provides crucial benefits in maintaining longitudinal structural integrity and preventing potential water infiltration at segment joints.

5.2.2 Joint Opening Analysis

A comparison of joint openings under different reinforcement conditions is presented in Fig. 13. When the ground surface surcharges were 30 and 50 kPa, the joint openings in the tunnel reinforced with steel plates spanning circumferential joints were larger than those of the unreinforced one. However, when the ground surface surcharges were 76.5 and 100 kPa, the joint opening in the tunnel reinforced with steel plates spanning circumferential joints was reduced by 7.48% and 12.29%, respectively, in comparison to those of the unreinforced one.

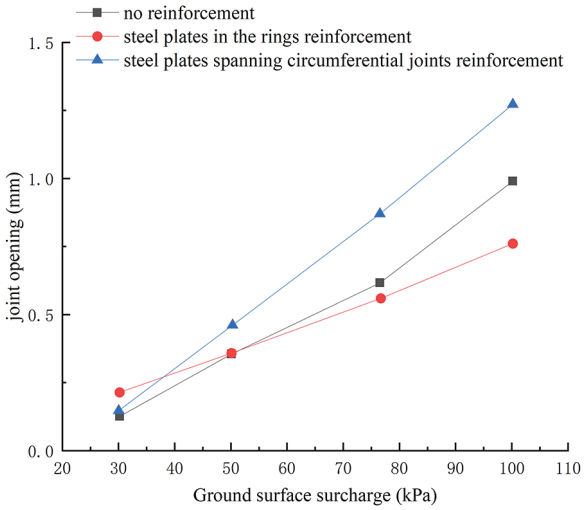

Figure 13: Comparison of joint openings under different dislocation conditions.

It is reported that most conventional internal reinforcement methods cannot effectively control joint openings between rings. The reinforcement of the tunnel with steel plates spanning circumferential joints restricted the displacement between two rings from the inside of the tunnel segments. However, this technique could not control joint openings between two rings caused by the external force on the outside of the tunnel segments. The steel plates in the rings mainly played a role in controlling the transverse deformation of the tunnel and increased the rigidity of the rings.

Under low surcharge conditions, the joint opening of tunnels reinforced with cross-joint steel plates was slightly greater than that of the unreinforced tunnel. This may relate to the initial contact state and stiffness activation process. At low stress levels, local constraints introduced by the plates can make the structure more sensitive to small deformations, while the composite action between steel and concrete has not yet been fully mobilized; as a result, the initial stiffness is not fully developed, causing a slight increase in opening. At higher surcharge levels, the composite action between steel plates and concrete becomes fully effective. The tensile strength and stiffness of the steel are fully activated, effectively limiting further joint opening. Cross-joint plates, acting as continuous reinforcement across the joints, significantly enhance the bending stiffness and tensile resistance of the inter-ring connection, leading to better deformation control compared to the unreinforced case.

For annular plate reinforcement, the joint opening tends to increase relative to the unreinforced tunnel as the surcharge grows. This is likely because annular plates primarily enhance the stiffness of individual rings but do not directly strengthen the ring-to-ring connection. As external loads increase, the rings themselves become stiffer, but the joints remain relatively weak, causing deformation to localize at the interfaces and resulting in greater opening. This non-monotonic behavior is consistent with mechanical mechanisms such

as progressive stiffness development in composite members, redistribution of internal forces, and the transfer of weak points under increasing loads.

5.3 Tunnel Settlement Analysis

The tunnel settlement occurred in the center of the top and bottom of the segment arch under the center of the ground surface surcharge, and the radial deformation of the bottom of the tunnel arch reflected the co-deformation of the tunnel with the soil body. It is observable from Fig. 14 that when the ground surface surcharges were 30, 50, 76.5, and 100 kPa, under the reinforcement with steel plates in the rings, the radial deformation at the bottom of the tunnel arch increased by 17.29%, 14.62%, 11.26%, and 31.32%, respectively, in comparison to those of the unreinforced one. Furthermore, when the ground surface surcharges were 30, 50, 76.5, and 100 kPa, under the reinforcement with steel plate spanning circumferential joints, the radial deformation at the bottom of the tunnel arch decreased by 39.96%, 36.12%, 32.97%, and 31.25%, respectively, in comparison to those of the unreinforced one.

After adding annular steel plates inside the rings, the radial deformation at the tunnel invert showed a slight increase. This phenomenon is mainly associated with stiffness redistribution and internal force adjustment. By increasing the local stiffness of each individual ring, the reinforcement can cause load to be redistributed toward the ring joints or relatively weaker zones, resulting in localized deformation concentration. In addition, the increased material stiffness contrast between reinforced and unreinforced components may reduce composite action efficiency, leading to slightly larger deformation responses at certain measurement points.

This behavior is consistent with the deformation redistribution mechanism observed in structures with abrupt stiffness transitions and suggests that further optimization of reinforcement schemes—especially combined with direct joint strengthening—could mitigate such localized effects.

The deformation patterns illustrated in Fig. 14b reveal that circumferential joint reinforcement produces contrasting effects in different tunnel regions. Beneath surface loads, the technique effectively controls radial displacement at the arch base, while in adjacent unloaded sections, minor deformation increases occur due to longitudinal stiffness enhancement. However, with maximum unloaded-zone deformations under 5 mm, the system proves highly effective in mitigating overall settlement, demonstrating its value despite localized behavioral variations.

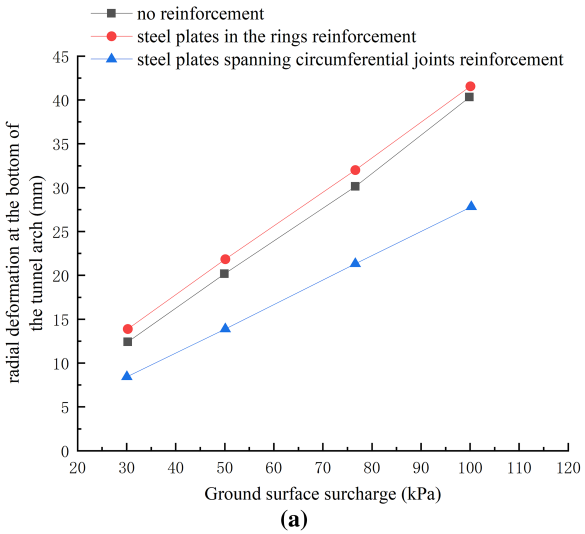

(a)

Figure 14: (Continued)

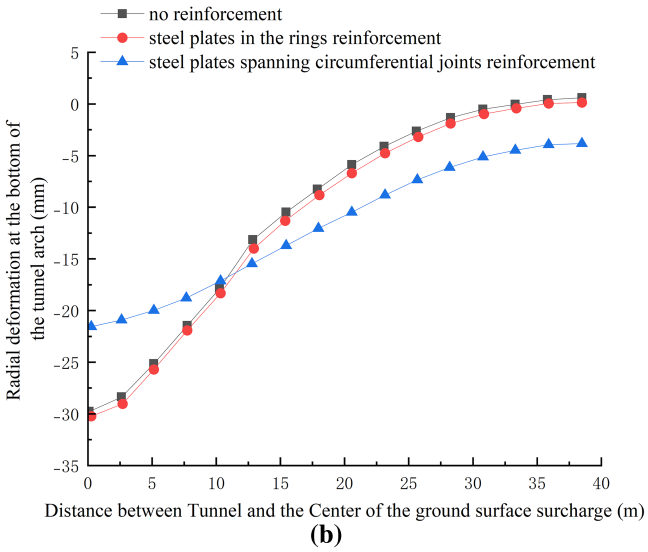

Figure 14: Comparison of radial deformations at the bottom of the tunnel arch. (**a**) Settlement of the tunnel arch bottom with different reinforcement methods under different ground surface surcharges, (**b**) Radial deformations at the bottom of the tunnel arch under different reinforcement conditions at 76.5 kPa.

The observed variation in deformation response along the tunnel is fundamentally driven by changes in longitudinal stiffness and the resulting redistribution of internal forces caused by steel plates installed at the circumferential joints. Under the surface surcharge, these joint plates markedly increase bending continuity between rings, effectively restraining joint opening and inter-ring dislocation and thereby reducing radial displacement at the arch invert. Mechanically, the plates establish continuous moment-transfer paths at the joints that diffuse local loads into adjacent segments and enhance the bearing capacity of the reinforced region. However, this local stiffening also modifies the longitudinal stiffness profile of the tunnel, creating a stiffness gradient between the loaded zone and neighboring unloaded sections. During the transfer of longitudinal bending moments and shear forces, stress is redistributed at these stiffness discontinuities and a portion of deformation is therefore transferred into adjacent, relatively more compliant segments, producing slight deformation increases there. This behaviour is consistent with a "stiffness-attraction" effect, whereby stiffer regions attract greater internal forces and thereby induce deformation accommodation in adjacent softer regions. Although the deformation increase in the unloaded sections is only on the order of millimetres, the joint plates substantially suppress deformation in the critically loaded zones; consequently, the overall effect of the local stiffness enhancement on tunnel deformation control is strongly positive.

5.4 Stress Distributions in the First Two Rings of the Staggered Tunnel Segment and Steel Plates under the Ground Surface Surcharge

The shear stress states of the first two rings of the staggered tunnel segment and the steel plates under the ground surface surcharge were found to be different. The shear stress states of the first two rings of the tunnel segment reinforced by two different methods under the ground surface surcharge of 76.5 kPa are compared in Fig. 15 (the capping block K was located at an angle of 18° to the right rotation).

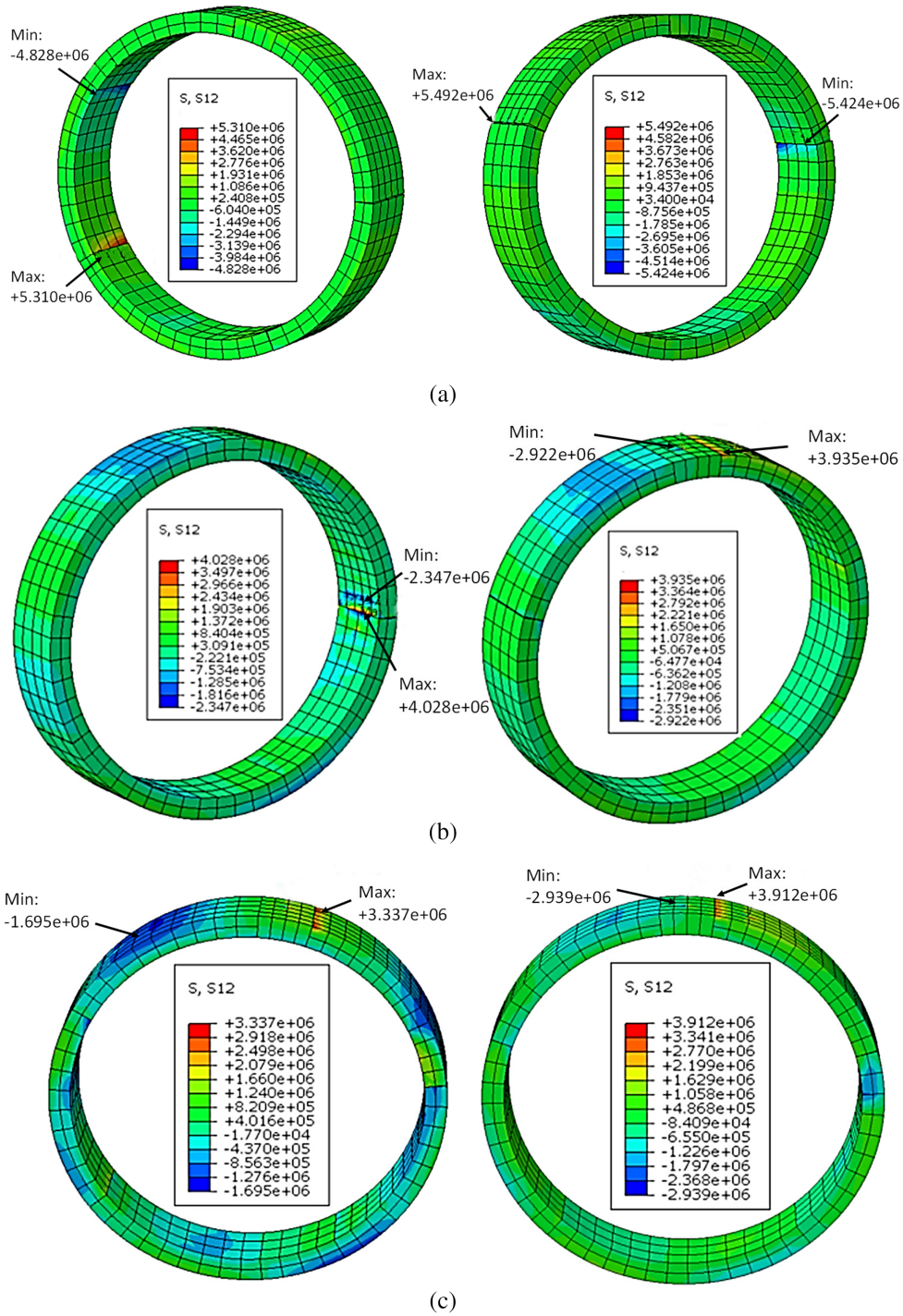

Figure 15: Comparison of shear stress distributions in the first and second rings of the tunnel segment under the ground surface surcharge. (**a**) Shear stress distribution in the first and second rings of the tunnel segment reinforced with steel plates in the rings under the ground surface surcharge, (**b**) Shear stress distribution in the first and second rings of the tunnel segment reinforced with steel plates in the rings under the ground surface surcharge, (**c**) Shear stress distributions in the first and second rings of the tunnel segment reinforced with steel plates spanning circumferential joints under the ground surface surcharge.

Fig. 15 demonstrates the effectiveness of cross-joint steel plate reinforcement in controlling lateral deformations under sustained surface loading conditions. This reinforcement technique substantially decreased inter-segment shear displacement, with peak shear stresses measured at 3.337 MPa in the initial ring (located at the K-B1 block interface) and 3.912 MPa in the subsequent ring (at B1 block position). These values represent significant reductions compared to the shear stresses observed in unreinforced tunnel sections, confirming the system's ability to improve structural performance under load.

The stress patterns illustrated in Fig. 16 reveal distinct mechanical behavior in the initial two rings of the staggered tunnel assembly under surface loading. In the primary ring (positioned diagonally above the tunnel), peak stresses developed at the right haunch longitudinal connection, while secondary ring plating exhibited maximum stresses at the contralateral left haunch joint. Stress analysis demonstrated concentrated shear transfer at segment interfaces, with the first ring's steel plating reaching 2.419 MPa at the right haunch and the subsequent ring showing a reduced maximum of 1.433 MPa at the left haunch—indicating both a magnitude decrease and spatial shift in critical stress locations between adjacent rings.

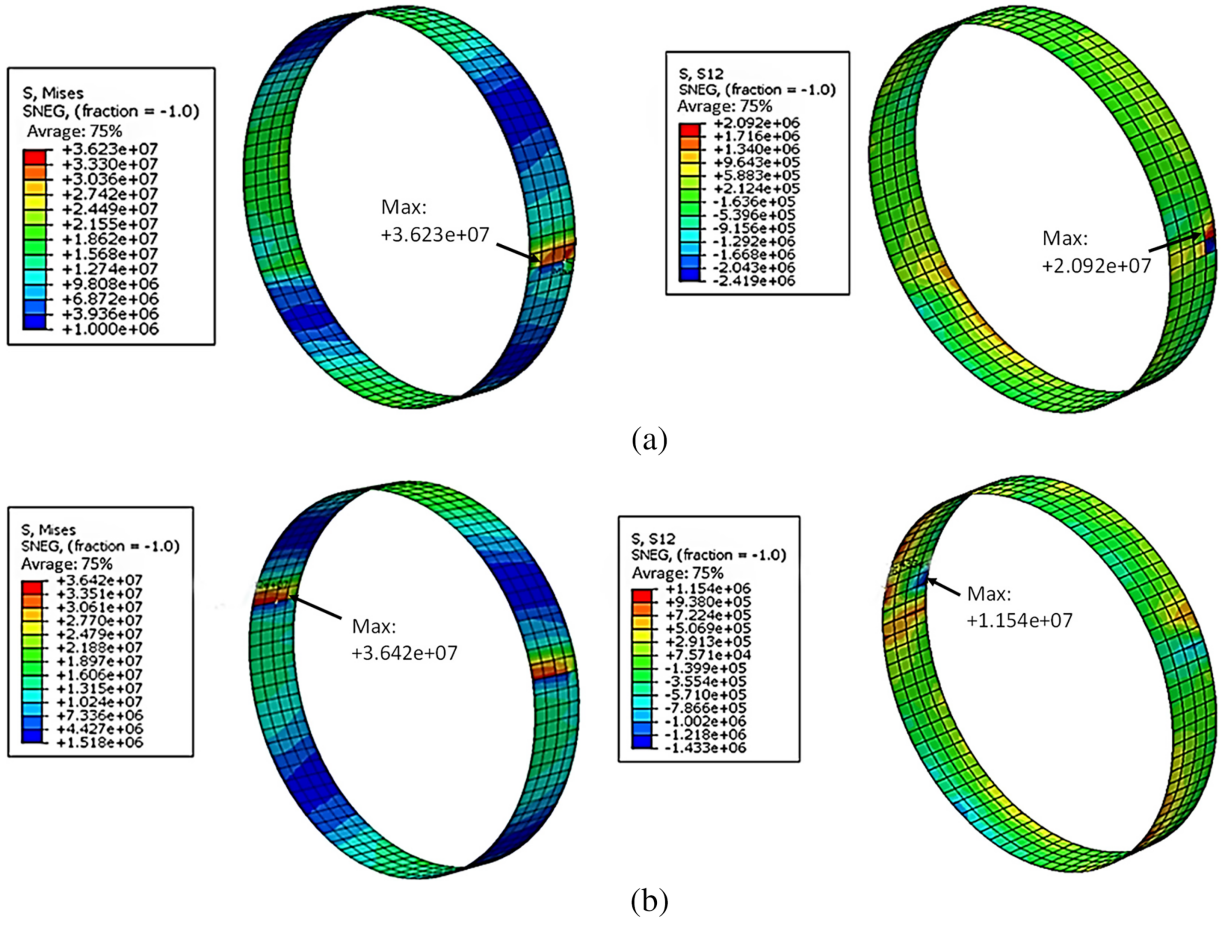

Figure 16: Comparison of stress distributions in steel plates in the first two rings of the staggered tunnel segment under the ground surface surcharge. (**a**) Stress distribution in the steel plate in the first ring of the tunnel segment, (**b**) Stress distribution in the steel plate in the second ring of the tunnel segment.

Fig. 17 illustrates the mechanical behavior of cross-joint steel plate reinforcement under surface loading conditions. The inter-ring connection system exhibited distinct stress characteristics at longitudinal joints of adjacent tunnel segments, with significantly higher shear stresses observed compared to annular plating

systems. Stress analysis revealed maximum values of 30.320 MPa at the left haunch and 2.864 MPa at the right haunch, demonstrating the system's capacity to assume greater shear transfer responsibilities from tunnel segments due to its strategic placement between rings.

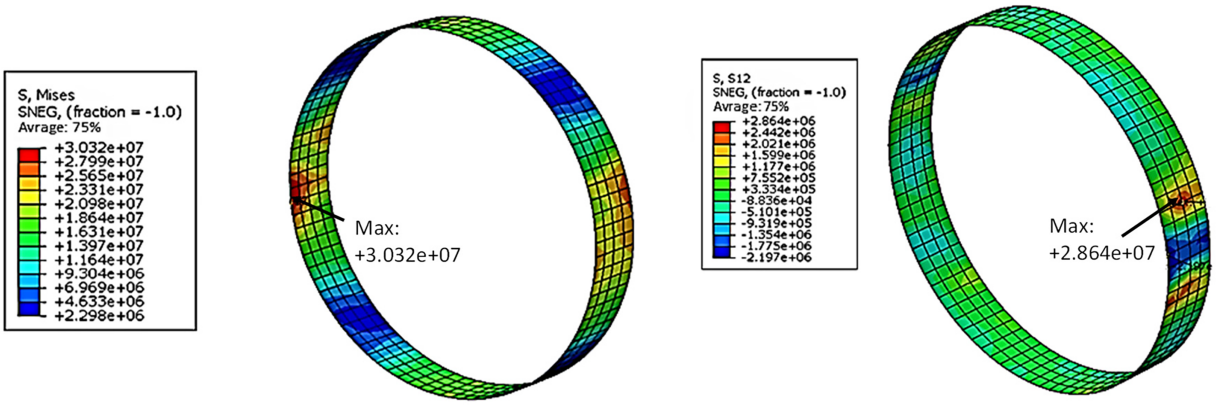

Figure 17: Stress distribution in the steel plate spanning circumferential joints in the staggered tunnel segment under the ground surface surcharge.

The cross-joint steel plate reinforcement system demonstrates superior performance in mitigating shear-induced displacements at tunnel haunch locations compared to conventional annular plating methods. This enhanced constraint capability effectively preserves both the structural integrity of the reinforcement system itself and the overall stability of the tunnel infrastructure.

6 Conclusions

The deformation control abilities of two different prestrengthening methods under different ground surface surcharge conditions were compared. The main observations of this work are presented below.

(1) The reinforcement with steel plates in the rings reduced the transverse deformation of the tunnel by increasing the stiffness in the ring direction; however, its effect on longitudinal deformation was limited. The dislocation between the rings of the tunnel was reduced by 20.96% compared with the unreinforced tunnel. In contrast, the joint opening and the radial deformation at the bottom of the tunnel arch under the reinforcement were 8.47% and 5.32% larger, respectively, than those of the unreinforced tunnel. Therefore, the reinforcement with steel plates in the rings had limited efficacy in controlling longitudinal deformation.

(2) The reinforcement with steel plates spanning circumferential joints reduced the transverse and longitudinal deformations of the tunnel. In particular, the reinforcement decreased the dislocations between the tunnel rings by 99.26% compared with the unreinforced tunnel. In addition, the radial deformation at the bottom of the tunnel was reduced by 26.97% compared with the unreinforced tunnel. Hence, the reinforcement with steel plates spanning circumferential joints increased the longitudinal stiffness of the tunnel.

(3) The reinforcement with steel plates spanning circumferential joints had a better shear stress control effect than the reinforcement with steel plates in the rings. Both reinforcement techniques reduced the shear stress of the tunnel segments under ground surface surcharges. The shear stress of the tunnel segments reinforced with steel plates in the rings was reduced by 26.25% in comparison to the unreinforced tunnel segments, whereas the shear stress of the tunnel segments reinforced with steel plates spanning circumferential joints was reduced by 32.96%.

(4) The numerical model did not consider factors such as long-term effects of soil, groundwater fluctuations, and steel plate fatigue. In the future, more advanced constitutive models, interface elements, and long-term monitoring data can be introduced to improve comparison and verification.

Acknowledgement: Not applicable.

Funding Statement: This work supported by "the Liaoning Provincial Department of Education Project (LJKZZ20220080)".

Author Contributions: Pengfei Zhao: Supervision, conceptualization, methodology, project administration, funding acquisition, writing—review & editing. Youlin Ye: Writing—original draft, investigation, visualization, formal analysis, data curation. All authors reviewed and approved the final version of the manuscript.

Availability of Data and Materials: Some or all data, models, or code generated or used during the study are available from the corresponding author by request.

Ethics Approval: Not applicable.

Conflicts of Interest: We declare that we have no financial and personal relationships with other people or organizations that can inappropriately influence our work, there is no professional or other personal interest of any nature or kind in any product, service and/or company that could be construed as influencing the position presented in, or the review of, the manuscript entitled "Transverse and longitudinal deformation control of a shield tunnel under ground surface surcharge conditions based on the Mohr-Coulomb model". The authors declare no conflicts of interest to report regarding the present study.

References

1. Wang HN, Chen XP, Jiang MJ, Song F, Wu L. The analytical predictions on displacement and stress around shallow tunnels subjected to surcharge loadings. Tunn Undergr Space Technol. 2018;71:403–27. doi:10.1016/j.tust.2017.09.015.
2. Huang Z, Zhang H, Fu H, Ma S, Liu Y. Deformation response induced by surcharge loading above shallow shield tunnels in soft soil. KSCE J Civ Eng. 2020;24(8):2533–45. doi:10.1007/s12205-020-0404-8.
3. Wei G, Zhang S, Xiang P. Model test study on the influence of ground surcharges on the deformation of shield tunnels. Symmetry. 2021;13(9):1565. doi:10.3390/sym13091565.
4. Han H, Zhang W, Wu Z, Sun W. Probabilistic analysis of tunnel deformation and ground surface settlement induced by surcharge in spatially variable soil. Comput Geotech. 2025;186:107369. doi:10.1016/j.compgeo.2025.107369.
5. Wei L, Yang C, Chen W, Liu L, Su D. Numerical analysis of ground surcharge effects on deformation characteristics in shield tunnel linings. Appl Sci. 2024;14(6):2328. doi:10.3390/app14062328.
6. Xiang P, Wei G, Jiang H, Ding Y, Guo H, Zhang R. Experimental study and theoretical analysis of the effect of surcharge/unloading at both sides of the ground surface on an existing shield tunnel at different burial depths. Buildings. 2023;13(8):1911. doi:10.3390/buildings13081911.
7. Yuan Y, Liu S, Xu Z, Wang X, Zia SMM, Zhang JL. Experimental investigation of the effect of ground surcharge on the structural behavior of a quasi-rectangular tunnel. Front Struct Civ Eng. 2025;19(3):427–44. doi:10.1007/s11709-025-1148-9.
8. Lee KM, Hou XY, Ge XW, Tang Y. An analytical solution for a jointed shield-driven tunnel lining. Num Anal Meth Geomechanics. 2001;25(4):365–90. doi:10.1002/nag.134.
9. Wu HN, Shen SL, Yang J, Zhou A. Soil-tunnel interaction modelling for shield tunnels considering shearing dislocation in longitudinal joints. Tunn Undergr Space Technol. 2018;78:168–77. doi:10.1016/j.tust.2018.04.009.

10. Liu X, Jiang Z, Yuan Y, Mang HA. Experimental investigation of the ultimate bearing capacity of deformed segmental tunnel linings strengthened by epoxy-bonded steel plates. Struct Infrastruct Eng. 2018;14(6):685–700. doi:10.1080/15732479.2017.1354892.
11. Qin Y, Zhang Y, Liu Z, Liu X. Experimental and analytical investigation of the mechanical behavior of deformed segmental tunnel linings strengthened by stainless steel corrugated plate. Tunn Undergr Space Technol. 2025;157:106355. doi:10.1016/j.tust.2024.106355.
12. Liu TJ, Chen SW, Lin PQ, Liu HY. Failure mechanism and strengthening effect of shield tunnel lining reinforced by steel plates with corbels. Eur J Environ Civ Eng. 2022;26(4):1603–21. doi:10.1080/19648189.2020.1717636.
13. Liu D, Huang H, Yue Q, Xue Y, Wang M. Behaviour of tunnel lining strengthened by textile-reinforced concrete. Struct Infrastruct Eng. 2016;12(8):964–76. doi:10.1080/15732479.2015.1076009.
14. Tengilimoglu O, Akyuz U. Experimental study on hybrid precast tunnel segments reinforced by macro-synthetic fibres and glass fibre reinforced polymer bars. Tunn Undergr Space Technol. 2020;106:103612. doi:10.1016/j.tust.2020.103612.
15. Wei G, Zhou X, Xu T, Zhang Y, Yao Z, Feng S. Full-scale experimental and structural characterization study of shield tunnel reinforcement under ground stacking loads. Structures. 2024;60:105865. doi:10.1016/j.istruc.2024.105865.
16. Liu D, Guo Y, Yao X. Interfacial behaviour of shield tunnel segment strengthened by thin plate at inner surface. Adv Mater Sci Eng. 2022;2022:7715844. doi:10.1155/2022/7715844.
17. JGJ/T 317-2014. Ministry of Housing and Urban-Rural Development of the People' s Republic of China (MOHURD). Technical specification for safety protection of urban rail transit structures. Beijing, China: Architecture & Building Press; 2014.
18. Wang S, Wang X, Chen B, Fu Y, Jian Y, Lu X. Critical state analysis of instability of shield tunnel segment lining. Tunn Undergr Space Technol. 2020;96:103180. doi:10.1016/j.tust.2019.103180.